Simulation of Self-Heating and Contact Resistance Influences on nMOSFETs

K. Matsuzawa, H. Kawashima[1], and K. Ouchi [1]
Advanced LSI Technology Laboratory, Toshiba Corporation
8, Shinsugita-cho, Isogo-ku, Yokohama 235-8522, Japan
Phone: +81-45-770-3693, Fax: +81-45-770-3578,
E-mail: kazuya.matsuzawa@toshiba.co.jp
1) Semiconductor Company, Toshiba Corporation

Abstract- **The lattice heat equation and the Schottky contact model were implemented in a device simulator to evaluate influences of self-heating on inversion layer mobility μ_{inv} and contact resistance R_{co} in scaled-down nMOSFETs. It is shown that the self-heating degrades μ_{inv} and reduces R_{co} of source/drain silicide. As ambient temperature T_{amb} increases, the degradation of μ_{inv} becomes more pronounced, because of the different contribution of the temperature dependence of the phonon scattering in the μ_{inv} model. Conversely, the reduction of R_{co} by the self-heating becomes more pronounced as T_{amb} decreases.**

I. INTRODUCTION

Influences of self-heating and contact resistance on electric characteristics could become pronounced as semiconductor devices are scaled down. The non-isothermal effect on MOSFETs has been studied [1], and the effect of the contact resistance on silicided nMOSFETs has been simulated by using a Schottky contact model [2]. However, electrical characteristics including both the self-heating and the contact resistance have not been investigated.

In this work, the lattice heat equation as well as the Schottky contact model have been implemented in the device simulator DIAMOND. It is demonstrated that the self-heating has two different effects on nMOSFETs with $CoSi_2$ silicided structure: one is increase of channel resistance and another is reduction of contact resistance.

II. PHYSICAL MODELS

Fig. 1 shows the device structure used in the present simulation. $CoSi_2$ silicide is attached to source/drain n^+ regions. The lattice heat equation was solved to obtain

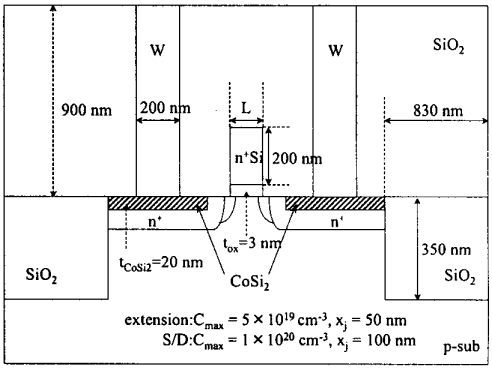

Figure 1: Schematic of simulated nMOSFET structure with $CoSi_2$ silicide in source/drain regions.

the distribution of the lattice temperature:

$$C_L \frac{\partial T_L}{\partial t} + \nabla \cdot \vec{S_L} = H, \tag{1}$$

$$\vec{S_L} = -\kappa_L \nabla T_L, \tag{2}$$

where C_L is the heat capacitance [$JK^{-1}cm^{-3}$], T_L the lattice temperature, $\vec{S_L}$ the heat flux, H the Joule heat, and κ_L the thermal conductivity. Lattice-temperature-dependence of κ_L for Si, SiO_2, $CoSi_2$, and W, composing the simulated nMOSFETs, was implemented to reproduce measurements [3][4], as shown in Fig. 2. Lattice-temperature-dependence of C_L was also modeled by using measurements [3][4]. The distribution of T_L was fed back to the intrinsic carrier concentration [5] and the mobility [6][7]. It was also fed back to the Schottky contact model [2] to introduce T_L dependence of the contact resistance.

Fig. 3 shows the schematic band diagram at the metal/semiconductor interface. Tunneling current density J_{TL} is calculated by the following equations [2]:

0-7803-6279-9/00/$10.00 © 2000 IEEE

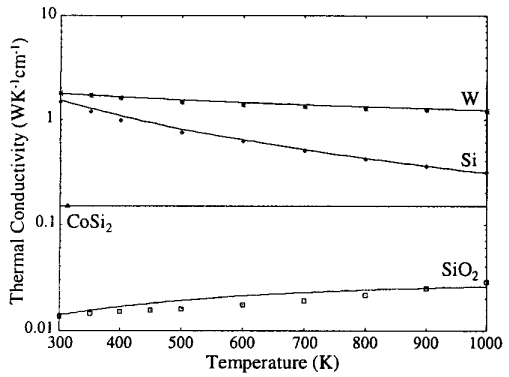

Figure 2: Lattice temperature dependences of thermal conductivities for materials composing the simulated structure of nMOSFET. Symbols are measurement: Si [3], SiO_2 [3], W [3], $CoSi_2$ [4]. Lines are present models.

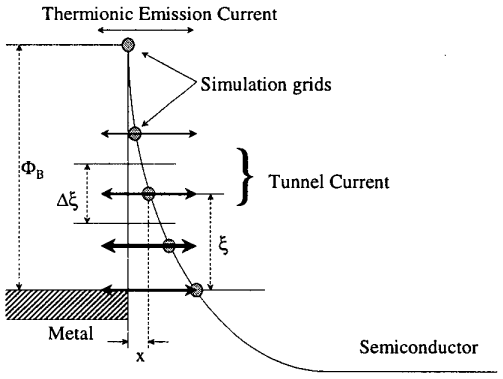

Figure 3: Schematic band diagram at the metal/semiconductor interface showing treatment of thermionic emission and tunneling.

$$J_{TL}(x) = \frac{A^*T}{k_B}\int_{\xi-\frac{\Delta\xi}{2}}^{\xi+\frac{\Delta\xi}{2}} D(\xi) ln(\frac{1+f_S(\xi)}{1+f_M(\xi)})d\xi, \quad (3)$$

$$D(\xi) = exp\left(-\frac{4\sqrt{2m^*}(q\phi_B-\xi)^{1.5}}{3\hbar q|E|}\right), \quad (4)$$

$$\xi = -q\psi, \quad (5)$$

$$\xi_{fM} = -q\psi_0 - q\phi_B, \quad (6)$$

$$\xi_{fS} = \xi - \frac{\xi_{gap}}{2} + k_BTln\frac{n}{n_i}, \quad (7)$$

$$E = -\frac{\psi-\psi_0}{x}, \quad (8)$$

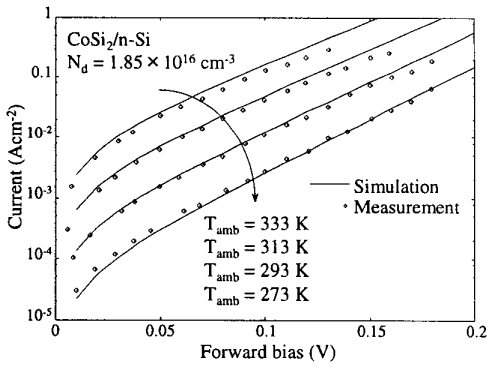

Figure 4: Influence of ambient temperature T_{amb} on $CoSi_2$ Schottky barrier diode under forward bias conditions.

where x is the distance from the interface, A^* [$Acm^{-2}K^{-2}$] the Richardson constant, T the electron temperature assumed to be equal to T_L, k_B Boltzmann's constant, ξ the electron energy, $\Delta\xi$ the energy difference in the control volume specified by discretization grids, D the tunneling probability ($D = 1$ for the thermionic emission), m^* the effective mass, q the elementary charge, ϕ_B the barrier height, $\hbar$ the reduced Planck constant, E the average electric field, ψ the potential at each grid, ψ_0 the potential at the interface, ξ_{gap} the energy band gap of the semiconductor, n the electron concentration, and n_i the intrinsic carrier concentration. Although f_S and f_M are the Maxwell-Boltzmann distribution functions in the semiconductor and in the metal, the degenerate effect is incorporated by using (3). ξ_{fM} and ξ_{fS} are the Fermi energy used in f_M and f_S respectively. ϕ_B and A^* for electrons, important parameters in the Schottky contact model, are 0.64 eV and 67 $Acm^{-2}K^{-2}$, which were determined to reproduce measurements of the ambient temperature T_{amb} dependence of the forward bias characteristics for $CoSi_2$ Schottky barrier diodes [8], as shown in Fig. 4.

Fig. 5 shows impurity concentration dependence of the contact resistance R_{co}. Since contacts of actual nMOSFETs are usually attached to high impurity concentration regions, the bandgap narrowing effect [9] and the Fermi-Dirac energy distribution should be incorporated into the Schottky contact model. The former has the effect making R_{co} lower and the latter makes it higher. The influence of T_{amb}, also plotted in Fig. 5, shows that R_{co} is lower under higher T_{amb}. In high impurity concentration regions, discrepancy with measurements [10][11] seems to become larger. R_{co} might be underestimated in such region. However, since the impurity concentration around contacts is below 10^{20} cm^{-3} in the present simulations, we suppose that simulation results are adequate.

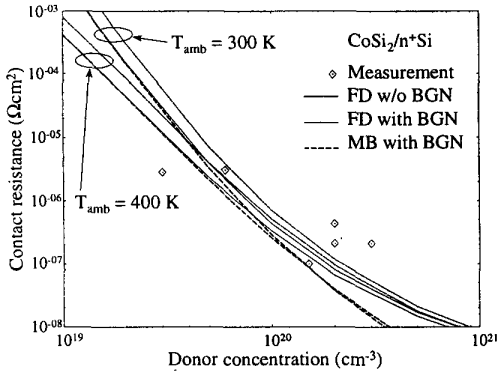

Figure 5: Influences of BGN (bandgap narrowing), difference between FD (Fermi-Dirac) and MB (Maxwell-Boltzmann) statistics, and the ambient temperature T_{amb} on $CoSi_2$ contact resistance.

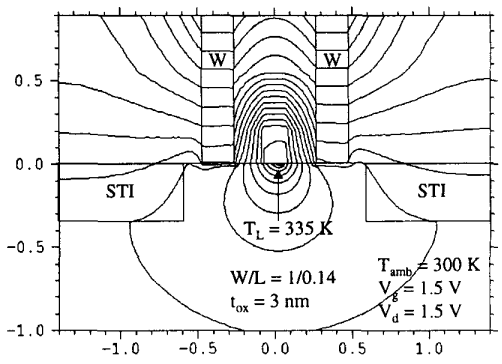

Figure 6: Lattice temperature distribution in the nMOSFET structure with $CoSi_2$ silicide in source/drain regions under the ambient temperature T_{amb} =300 K , $V_g = V_d$ =1.5 V.

III. SIMULATION OF NMOSFETS

Fig. 6 shows a lattice temperature distribution in 0.14 μm gate nMOSFET structure. The heat sink regions are the top of source/drain electrodes and the bottom of the substrate. The thickness of the substrate is 10 μm. Fig. 7 shows transient characteristics of drain current I_d versus drain voltage V_d. Solid lines show currents calculated under non-isothermal condition, I_{noniso}, where the lattice heat equation is solved, whereas broken lines show currents under isothermal condition, I_{iso}. Under the condition without R_{co}, I_{noniso} becomes smaller than I_{iso} as V_d increases, because the channel resistance R_{ch} increases by the self-heating, namely, the phonon scattering probability in the inversion layer mobility μ_{inv} increases. Moreover, I_{noniso} becomes smaller than I_{iso} as T_{amb} is higher. This can be explained by the reduction rate of the mobility. Fig. 8 shows the mobility ratio of μ_{inv} under the non-isothermal condition to μ_{iso} under the isothermal condition at the substrate surface. In the channel region, the ratio is reduced as T_{amb} is higher. This is due to the different contribution of the temperature dependence of the phonon scattering in the μ_{inv} model. Fig. 9 schematically shows the contribution of each scattering mechanism in μ_{inv}. The range of the effective electric field where the phonon scattering is dominant becomes wider as T_{amb} is higher. Therefore, I_{noniso} becomes more sensitive to the self-heating in Fig. 7.

On the other hand, the degradation of I_{noniso} by the self-heating becomes smaller under the condition with R_{co} in Fig. 7. This is because the temperature dependence of R_{co} is opposite to that of the phonon scattering. Fig. 10 shows the channel length dependence of the current ratio of $\frac{I_{noniso}}{I_{iso}}$. Influences of T_{amb} and R_{co} are clearly observed. The ratio considering R_{co} under $T_{amb} = 400K$ is closer to unity, because the reduction of R_{co} by the self-heating compensates for the increase of the channel resistance R_{ch}. Under $T_{amb} = 300K$, the current ratio considering R_{co} becomes slightly larger than unity in the short channel region. This is because the heat in the channel propagates to the contacts more as the channel length is smaller and the reduction of R_{co} exceeds the increase of R_{ch}.

IV. CONCLUSION

The lattice heat equation as well as the Schottky contact model have been implemented in the device simulator. Using the simulator, it is shown that two effects of the self-heating, the increase of R_{ch} and the reduction of R_{co}, can be simulated quantitatively.

ACKNOWLEDGMENT

The authors wish to thank Dr. S. Takagi for his valuable comments.

REFERENCES

[1] H. Kawashima and R. Dang, "Non-isothermal device simulation of gate switching and drain breakdown characteristics of Si MOSFET in transient state," IEICE Trans. Electron. vol. E82-C, P. 894, 1999.

[2] K. Matsuzawa, K. Uchida, and A. Nishiyama, "A unified simulation of Schottky and ohmic contacts," IEEE

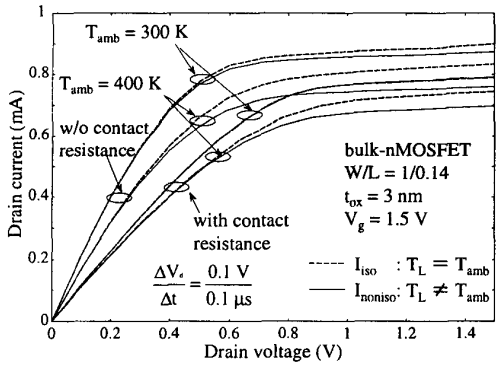

Figure 7: Drain current versus drain voltage to demonstrate influences of the self-heating, the ambient temperature T_{amb}, and the contact resistance R_{co}.

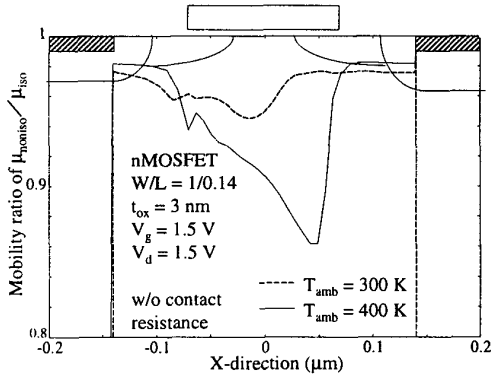

Figure 8: Distribution of mobility ratio of μ_{noniso} to μ_{iso} at the substrate surface.

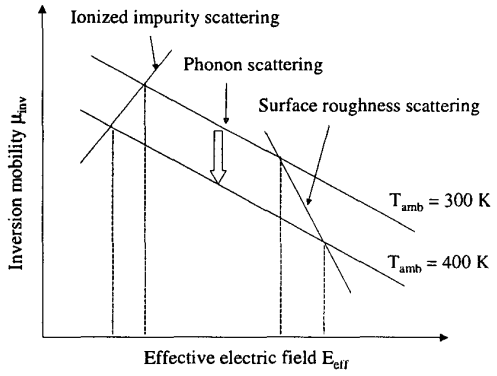

Figure 9: Schematic of effective electric field dependence of μ_{inv}.

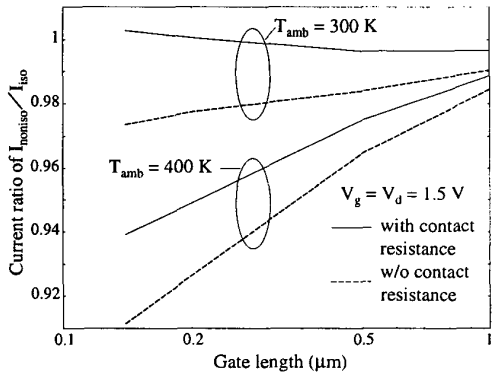

Figure 10: Drain current ratio of I_{noniso} to I_{iso} versus gate length.

Trans. Electron Devices, vol. 47, p. 103, 2000.
[3] Y. S. Touloukian et al., in Thermophysical Properties of Matter, vol. 1, 2, 4, 5, IFI/Plenum, 1970.
[4] N. G. Einspruch and G. B. Larrabee, "Materials and Process Characterization," VLSI Electronics Microstructure Science, vol. 6, Academic Press, 1983.
[5] M. A. Green, "Intrinsic concentration, effective densities of states, and effective mass in silicon," J. Appl. Phys., vol. 67, p. 2944, 1990.
[6] D. B. M. Klaassen, "A unified mobility model for device simulation - II. Temperature dependence of carrier mobility and lifetime," Solid-State Electron., vol. 35, p.961, 1992.
[7] C. Jacoboni, C. Canali, G. Ottaviani, and A. A. Quaranta, "A review of some charge transport properties of silicon," Solid-State Electronics, vol. 20, p. 77, 1977.
[8] A. Lauwers, A. Vercaemst, M. Van Hove, K. Kyllesbech Larsen, R. Verbeeck, R.Van Meirhaeghe, K. Maex, and M. Van Rossum, "Electrical characterisation of epitaxial (100) $CoSi_2$/Si contacts obtained using a Ti/Co bilayer," Mat. Res. Soc. Symp. Proc., vol. 320, p. 59, 1994.
[9] N. Shigyo, N. Konishi, and H. Satake, "An improved bandgap narrowing model based on corrected intrinsic carrier concentration," IEICE Trans. Electron., vol.E75-C, p. 156, 1992.
[10] INSPEC, "Property of silicon," 4, ser. EMIS Datareviews Series, 1988.
[11] V. Probst, H. Schaber, A. Mitwalsky, H. Kabza, B. Hoffmann, K. Maex, and L. van D. Hove, "Metal-dopant-compound formation in $TiSi_2$ and $TaSi_2$: Impact on dopant diffusion and contact resistance," J. Appl. Phys. vol. 70, p. 693, 1991.